

DISSERTATION

“RETINOTOPIC MECHANICS DERIVED USING CLASSICAL PHYSICS”

“RETINOTOPISCHE MECHANIKEN, DIE MIT KLASSEPHYSIK ABGELEITET WERDEN”

ZUR ERLANGUNG DES
AKADEMISCHEN GRADES DOCTOR
RERUM MEDICINALIUM (DR. RER.
MEDIC.)

VORGELEGT DER MEDIZINISCHEN
FAKULTÄT CHARITÉ –
UNIVERSITÄTSMEDIZIN BERLIN

VON

IFEDAYO-EMMANUEL ADEYEFA-OLASUPO

PROF.DR. HENRIK WALTER
DATUM DER PROMOTION:

ABSTRACT

The concept of a cell's receptive field is a bedrock in systems neuroscience, and the classical static description of the receptive field has had enormous success in explaining the fundamental mechanisms underlying visual processing. Borne out by the spatio-temporal dynamics of visual sensitivity to probe stimuli in primates, I build on top of this static account with the introduction of a new computational field of research, retinotopic mechanics. At its core, retinotopic mechanics assumes that during active sensing receptive fields are not static but can shift beyond their classical extent. Specifically, the canonical computations and the neural architecture that support these computations are inherently mediated by a neurobiologically inspired force field. For example, when the retina is displaced because of a saccadic eye movement from one point in space to another, cells across retinotopic brain areas are tasked with discounting the retinal disruptions such active surveillance inherently introduces. This neural phenomenon is known as spatial constancy. Using retinotopic mechanics, I propose that to achieve spatial constancy or any active visually mediated task, retinotopic cells, namely their receptive fields, are constrained by eccentricity dependent elastic fields. I propose that elastic fields are self-generated by the visual system and allow receptive fields the ability to predictively shift beyond their classical extent to future post-saccadic location such that neural sensitivity which would otherwise support intermediate eccentric locations likely to contain retinal disruptions is transiently blunted.

1. BACKGROUND

1.1. Predictive Neural Remapping

The concept of a brain cell or neuron's classical receptive field (cRF) is fundamental in systems neuroscience and has been immensely successful in explaining the basic mechanisms of perception. In fact, seven Nobel Prizes have been awarded to researchers studying cRF structure and function: Sherrington, Ramón y Cajal, Granit, Hartline, von Békésy, Hubel, and Wiesel [1]. However, a seminal paper published by Michael Goldberg and colleagues [2] challenged this classical static description of the cRF. In this study, the authors demonstrated that prior to a saccadic eye movement (SEM), cRFs can transiently shift their neural sensitivity toward their future post-saccadic location, almost as if they have shifted their spatial preference. This phenomenon is known as retinotopic remapping or what I will refer to here as predictive neural remapping (PNR). PNR, its translational form, has been proposed as a key mechanism that allows biological systems to maintain a stable and continuous perception of the visual world, despite the retinal displacement and motion blur that accompany each SEM. While this phenomenon has been replicated by other researchers, a study conducted by Tirin Moore, and colleagues reported that cRFs primarily shift their sensitivity toward spatial extents surrounding the saccade target, not their future post saccadic locations. This form of PNR is commonly referred to as convergent remapping [3].

Translational and convergent accounts of PNR remain at odds, and the functional role that these divergent forms of remapping play in mediating spatial constancy remains unresolved. Several critical questions persist. For instance, the high frequency of saccades (occurring approximately 2–4 times per second) and the associated cRF shifts may impose significant energetic demands. Yet, the fundamental principles governing how the brain balances energy expenditure with the need for predictive accuracy remain unclear. Additionally, the functional architecture that allows retinotopic cells to maintain or enhance sensitivity beyond their classical center-surround structure, while avoiding maladaptive forms of PNR remains a mystery.

1.2. Mathematical Overview

In the following sections, I will provide a very simple and concise overview of the most significant mathematical models related to PNR. Specifically, I will review prominent studies that exemplify these models and reference additional studies employing similar mathematical approaches, although different in their formulations. After discussing these models, I will briefly address their limitations. In Chapter 2, I will introduce my mathematical framework, “retinotopic mechanics” (RM), and its advantages.

1.2.1. Vector Subtraction Models

The first class of mathematical models employed by theorists to investigate PNR can be classified as vector subtraction models (VSMs). These models suggest that PNR involves the manipulation of mathematical vectors through subtractive operations. Specifically, retinotopic cells—whether encoding the upcoming SEM [4], efference copy signals [5][6], or velocity signals required for the eyes to reach the saccade target [7]—must have information that corresponds to the difference in magnitude between the saccade target and the current position of the eye. Using this information, cells across retinotopic brain areas (RBAs) can correctly predict and shift their neural response to their future post-saccadic locations.

Let $f(x\varphi, y\varphi, t)$ denote the response of a retinotopic cell at time t . If the cell correctly predicts the impending spatial extent of the saccade target, resulting in $f(x\varphi + \delta_x, y\varphi + \delta_y, t + \delta_t)$, at a future time $t + \delta_t$, then its response is invariant:

$$f(x\varphi + \delta_x, y\varphi + \delta_y, t + \delta_t) = f(x\varphi, y\varphi, t). \quad [\text{Eq.1}]$$

Expanding on [Eq.1], we can explicitly approximate this neural invariance $f(x\varphi + \delta_x, y\varphi + \delta_y, t + \delta_t)$ over some future time (δ_t) with respect to the displacement of a saccade target along the x and y direction. Specifically, δ_x and δ_y denotes the target displacement at the current time point t , where $\frac{\partial f}{\partial x}$ and $\frac{\partial f}{\partial y}$ represents the corresponding response gradient with respect to x and y [Eq. 2]. Consistent with [Eq.1], we can now directly observe that under certain conditions, for example small target displacements, the response of the cell (f) is negligible, consistent with the translational form of PNR.

$$f(x\varphi, y\varphi, t + \delta_t) = f(x\varphi, y\varphi, t) - (\delta_x) \cdot \frac{\partial f}{\partial x} - (\delta_y) \cdot \frac{\partial f}{\partial y} \quad [\text{Eq.2}]$$

Let's further assume that the saccade target is fixed, that is, no saccade displacement signal is present and that f is driven by signals that carry information about velocity ($\delta_x = -\delta_t \cdot v_x$; $-\delta_y = \delta_t \cdot v_y$). With this assumption, it is possible to modify [Eq.2], where in [Eq.3] changes over some time interval δ_t is the result of velocity signals (V_{xy}) coming from relevant RBAs. To then approximate the discrete dynamics for a given cell i , its future response - $f(x\varphi_i, y\varphi_i, t + \delta_t)$ can be computed as a weighted sum of activity of its neighboring cells j . Here the coefficients a_{ij} , b_{ij} and c_{ij} are weights that depend on the distance between i and j [Eq. 4].

$$f(x\varphi, y\varphi, t + \delta_t) = f(x\varphi, y\varphi, t) + \delta_t \left(V_x \cdot \frac{\partial f}{\partial x} + V_y \cdot \frac{\partial f}{\partial y} \right) \cdot \frac{\partial f}{\partial x} \cdot \frac{\partial f}{\partial y} \quad [\text{Eq.3}]$$

$$f(x\varphi, y\varphi, t + \delta_t) = \sum_j (a_{ij} + \delta_t \cdot V_x \cdot b_{ij} + \delta_t \cdot V_y \cdot c_{ij}) \cdot f(x_i + dx_j, y_i + dy_j, t) \quad [\text{Eq.4}]$$

1.2.2. Artificial Network Models

The second class of models which has also been used to investigate PNR are artificial network models (ANMs). These models typically include a recurrent hidden layer along with an input and output layer [8, 9, 10]. The input layer in general encodes information about the initial saccade target location. Thus, the neural activity at any spatial extent (x, y) in the retinotopic field is represented by $f(x, y)$, where x_0 and y_0 corresponds to the cells most strongly activated by the saccade target, while σ specifies the width of the response distribution. This central activity represents the area of the retina directly "viewing" the saccade target. Adjacent cells, which are less activated by the target, contribute to a gradient response profile. The spread of this response is modeled by a Gaussian:

$$f(x, y) = \exp \left(-\frac{(x-x_0)^2 + (y-y_0)^2}{2\sigma^2} \right) \quad [\text{Eq.5}]$$

Efference copy information about the saccade target is fed into the hidden layer, where it is encoded in one of three ways: as a transient signal about the impending SEM, a sustained signal the plans the SEM from the center of gaze to the saccade target, or a velocity signal. Let $h_{j(t+1)}$ represent the response of retinotopic cell - h_j at time $t+1$. The recurrent weights between cells within the hidden layer are denoted by w_{ij} , while $\varepsilon_{k(t)}$

and w'_{jk} represent the efference copy related signals from the input layer and their corresponding weights, respectively. With this architecture, cells in the hidden layer can adjust the internal representation that approximates the location of the saccade target, x_0, y_0 . This adjustment leads to an updated internal representation that accurately reflects the spatial extent of the target once the eye has landed.

$$h_{j(t+1)} = \phi(\sum_i w_{ij} h_{i(t)} + \sum_k w'_{jk} \varepsilon_{k(t)}) \quad [\text{Eq.6}]$$

The updated internal representation- x_0, y_0 , is made available to units within the output layer. Here, $\delta x, \delta y$ represents the impending displacement of the eyes. To assess whether the artificial network has accurately remapped to the target location, the updated internal representation is evaluated, where r_ε - the remapping error, is computed. Here ω denotes the predicted representation $\hat{\omega}$ is the correct representation. Because the aim of these models is to minimize r_ε through iterative adjustments (i.e. learning), the partial derivative of r_ε with respect to each weight in all layers — input, hidden, and output is computed. Here, $\frac{\partial r_\varepsilon}{\partial \omega}$ represents the derivative of the error with respect to ω and $\frac{\partial \omega}{\partial w_{ij}}$ represents the derivative of the predicted position with respect to w_{ij} . Over time, weights across all layers are updated using gradient descent, where w'_{ij} represents the updated weights and η denotes the learning rate used by the artificial network.

$$x_0' = x_0 + \delta x, \quad y_0' = y_0 + \delta y \quad [\text{Eq. 7}]$$

$$r_\varepsilon = \sqrt{\frac{1}{n} \sum_{j=1}^n (\omega_j - \hat{\omega}_j)^2} \quad [\text{Eq. 8}]$$

$$\frac{\partial r_\varepsilon}{\partial w_{ij}} = \frac{\partial r_\varepsilon}{\partial \omega_j} \cdot \frac{\partial \omega_j}{\partial w_{ij}} \quad [\text{Eq. 9}]$$

$$w'_{ij} = w_{ij} - \eta \frac{\partial r_\varepsilon}{\partial w_{ij}} \quad [\text{Eq. 10}]$$

1.2.3. Biologically Inspired Models

The third and last class of models typically used to investigate PNR I will refer to as biologically inspired models (BIMs). These models are biologically inspired because they are constrained by findings from psychophysical and neurophysiological (or biological) studies in primates [11,12,13]. Specifically, they assume that RBAs have a shared retinotopic map, reflecting the spatial layout of the retina. They further assume that visual processing is hierarchical, with lower-order RBAs (α) responsible for processing finer details through smaller cRFs, while higher-order RBAs (β), with larger cRFs, pool information from lower order areas to generalize across broader regions of the visual field. Each RBA is characterized by a magnification factor, reflecting a higher concentration of sensitized cells within the central 2 degrees of the visual field compared to the periphery. Let $r_i^{\alpha 1}$ represent the response of retinotopic cells, where S_p denotes the position of a saccade target with magnitude k . The term $c_i^{\alpha 1}$ indicates the center of a cell's cRF, whose density scales with eccentricity. Indeed, the activity of cell i decreases as the distance between the saccade target and cRFi increases [Eq.11].

$$r_i^{\alpha 1} = k \cdot \exp \left(\frac{-\|S_p - c_i^{\alpha 1}\|^2}{2(\sigma_i^{\alpha 1})^2} \right) \quad [\text{Eq. 11}]$$

As a new region of interest is selected, oculomotor feedback signals, the precursor to gain modulation signals [Eq. 12], provides crucial information about the consequence of the impending SEM. In this context, c^{SEM} denotes the SEM signal, as cells closer to the saccade target receive a stronger feedback signal, and those farther away receive a weaker signal. The feedback signal, modulated by $f(t)$, strengthens as the time to saccade onset approaches and declines shortly after.

$$\hat{r}_i^{\alpha} = \exp \left(\frac{-\|c_i^{\alpha 1} - c^{SEM}\|^2}{2(\sigma_i^{AE})^2} \right) \cdot f(t) \quad [\text{Eq.12}]$$

Once feedback signals emerge, a gain modulation is applied to the visual input, $r_i^{\alpha 1}$, leading to an amplified response around the saccade target:

$$r_i^{\lambda 1} = \frac{r_i^{\alpha 1} (1+k \cdot \hat{r}_i^{\alpha})}{1+k \cdot \max_j(r_j^{\alpha 1}) \cdot \hat{r}_i^{\alpha}} \quad [\text{Eq.13}]$$

The gain-modulated activity of cells in lower-order RBAs is eventually pooled, providing a spatially invariant representation in higher-order RBAs. Here, r_j^{φ} represents the pooled activity, which is dominated by the cell i with the largest gain-modulated response $r_i^{\lambda 1}$.

$$r_j^{\varphi} = \max_i \left(r_i^{\lambda 1} \cdot \exp \left(-\frac{\|c_i^{\alpha 1} - c_j^{\varphi 1}\|_2^2}{2(\sigma_j^{\varphi 1})^2} \right) \right) \quad [\text{Eq.14}]$$

1.3. Model Limitations

Despite the computational insights these three classes of models have provided, they exhibit four significant limitations. First, these models are highly parameterized and include non-modular components, with simulations ultimately conforming to specific experimental demands, that is, favoring one form of PNR over another. For example, VSMs and ANMs cannot account for the convergent form of PNR, while BIMs fail to explain the translational form of PNR. As a result, none of these models adequately account for the divergence in experimental findings. Second, the frequency of saccades and the accompanying predictive shifts in cRFs are energetically costly, yet these models fail to uncover a governing principle by which retinotopic cells balance energy expenditure with predictive function. Third, while the anatomical center-surround structure of cRFs is well established, none of these models propose a functional neural architecture that can explain how cRF shifts beyond their anatomical extent without leading to unsustainable forms of PNR. Finally, these models are neither general nor expressive enough, as they cannot account for afoveated biological systems who also make SEMs to orient themselves in the world.

2. METHOD

In this chapter, I will address the limitations of the models discussed in the previous chapter by introducing a fundamentally different mathematical framework (Retinotopic Mechanics). This framework is rooted in the principles and formalism of theoretical physics. Building upon this foundation, I will construct a general model in Chapter 3 that incorporates the new framework. Additionally, I will compare the model's predictions with both existing experimental data and psychophysical experiments that I have personally conducted.

2.1. Nonlinear Neural Spring Dynamics

Retinotopic mechanics assume that retinotopic cells routinely shift beyond their classical center-surround structure whenever the animal is moving, which includes cases when it is moving its eyes. Each cell does not behave like a simple thermometer, driven solely by the absence or presence of external perturbation. Nor does it behave like a perceptron. Instead, this framework posits that retinotopic cells behave computationally like a spring-loaded sensor that is governed by neural elastic fields ($\varepsilon l\varphi$'s).

2.1.1. Adaptive Elasticity

In the case where a cell's $\varepsilon l\varphi$ is adaptive, let \hat{x} represent the displacement of the neural sensor within its $\varepsilon l\varphi$, and k denote its spring constant. As \hat{x} approaches the boundary of its $\varepsilon l\varphi$, paradoxically the sensor ceases to respond despite the presence of external forces. Such inhibition by the sensor's $\varepsilon l\varphi$ prevent any unsustainable forms of PNR, such as over-translational shifts, ensuring cells across RBAs remain appropriately sensitive across the entire visual field.

$$\vec{F}_s = \begin{cases} -k\hat{x} & \text{if } |\hat{x}| \leq \varepsilon l\varphi \\ 0 & \text{if } |\hat{x}| > \varepsilon l\varphi \end{cases} \quad [\text{Eq.15}]$$

2.1.2. Maladaptive Elasticity

Conversely, a cell's $\varepsilon l\varphi$ can also become maladaptive in one of two ways, reflecting dynamics seen in patients with mental and psychiatric disorders [14 15]. Let τ represents the spring's delay in response, where the spring either fails to respond to external force (Fig 1B) or is unable to appropriately delay its response in the absence of external force.

$$\vec{F}_S = \begin{cases} -k\hat{x}(t - \tau) & \text{if } |\hat{x}(t - \tau)| \leq \varepsilon l\varphi \text{ and } t > \tau \\ 0 & \text{if } |\hat{x}(t - \tau)| > \varepsilon l\varphi \text{ or } t \leq \tau \end{cases} \quad [\text{Eq.16}]$$

The second way a spring's $\varepsilon l\varphi$ can become maladaptive is when the spring is displaced beyond its $\varepsilon l\varphi$. As the spring approaches its boundaries, it enters a non-linear regime, where the additional quadratic term $-\alpha(\hat{x} - \varepsilon l\varphi)^2$ starts to dominate, causing the spring to move beyond its $\varepsilon l\varphi$. In theory, this would require an increasingly larger force, but in a biological or maladaptive context, this force that is exerting its influence on the spring is hallucinated —akin to how a clinical patient might hallucinate the presence of an external cue when, in reality, no such external perturbation exists.

$$\vec{F}_S = \begin{cases} -k\hat{x} & \text{if } |\hat{x}| \leq \varepsilon l\varphi \\ -k\hat{x} - \alpha(\hat{x} - \varepsilon l\varphi)^2 & \text{if } |\hat{x}| > \varepsilon l\varphi \end{cases} \quad [\text{Eq.17}]$$

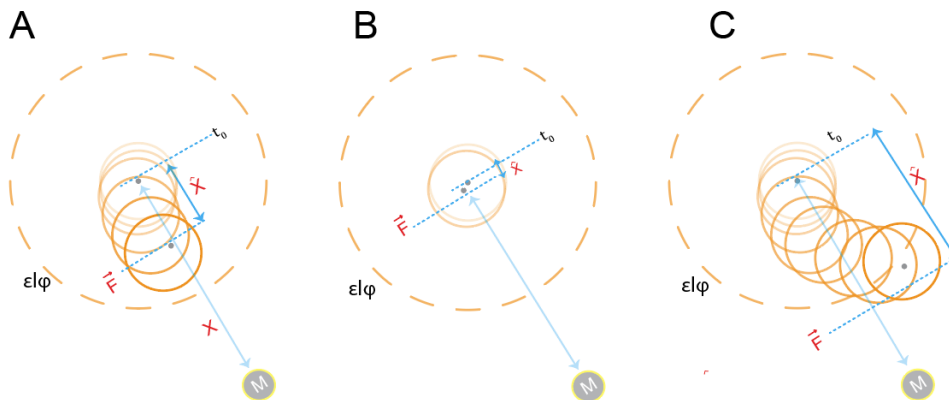


Figure.1 Non-linear Dynamics of Spring-Loaded Neural Sensors (own representation, Ifedayo-Emmanuel Adeyefa-Olasupo)

2.2. Differences in Design Principles

While foveated and afoveated biological systems make SEM to orient themselves within their environment, they have evolved with different design principles. These principles determine how retinotopic cells, and in turn their $\varepsilon\varphi$ s, tile visual space in the absence of external forces [16].

Let us assume each cRFs across RBAs actively modulate sensitivity across the visual field and is defined by two key parameters. The first parameter denoted as p_i represents the center location (x_i, y_i) of the cRF at time t_0 . The location p_i directly determines the cRF's eccentricity, represented as ecc_i . The second parameter is d_i , indicating the diameter of the cRF. In foveated biological systems d_i is a function of eccentricity ecc_i , where k represents the rate at which d_i scales with increasing eccentricity [Eq. 18]. In more dynamic cases, such as around the time of a SEM, d_i can vary over time, influenced by the rate of change of ecc_i [Eq. 19].

$$\frac{dd_i}{decc_i} = k \quad [\text{Eq.18}]$$

$$\frac{dd_i}{dt} = k \cdot \frac{decc_i}{dt} \quad [\text{Eq.19}]$$

As described in Section 2.1.1, each cRF possesses an $\varepsilon\varphi$. In biological systems with a fovea, $\varepsilon\varphi$ s is dependent on ecc_i . In this context, d_i is scaled globally by a factor Ψ , ensuring that the radius of $\varepsilon\varphi$ exceeds d_i , where $\Psi > 1$. This scaling ensures that the $\varepsilon\varphi$ expands appropriately with increasing ecc_i . In more dynamic scenarios, the rate of change of $\varepsilon\varphi$ overtime is directly related to the rate of change of ecc_i , with Ψ scaling this relationship, as shown in Eq. 21.

$$\varepsilon\varphi = \Psi \cdot d_i, \text{ where } \Psi > 1 \quad [\text{Eq.20}]$$

$$\frac{d\varepsilon\varphi}{dt} = \Psi \cdot \frac{dd_i}{dt} = \Psi \cdot k \cdot \frac{d(ecc_i)}{dt} \quad [\text{Eq.21}]$$

In contrast, in afoveated biological systems, the relationship is independent of ecc_i , meaning that the d_i remains constant regardless of variations in ecc_i .

Mathematically, this can be expressed as follows:

$$\frac{dd_i}{d(ecc_i)} = 0 \quad [\text{Eq.22}]$$

$$\frac{dd_i}{dt} = 0 \quad [\text{Eq.23}]$$

In such systems, similar to the foveated system, the $\varepsilon l\varphi$ can still be described by Eq. (21). However, since d_i is constant, $\varepsilon l\varphi$ also remains unchanged. Therefore, the rate of change of $\varepsilon l\varphi$ overtime is given by:

$$\frac{d\varepsilon l\varphi}{dt} = 0 \quad [\text{Eq.24}]$$

2.3. Retinotopic Mass

For cRFs to operate effectively within a force field such that they can move beyond their classical center-surround structure, the presence of what I term retinotopic mass (rm) is crucial. In this context, rm exhibits three distinct phases: growth, plateau, and decay (Fig 2, right panel). Let g represent the rate at which the mass appears, which could be either sudden or gradual, and let c be a scaling factor that modulates the overall magnitude of the growth rate. During the growth phase, the rate of change of retinotopic mass is described by:

$$\frac{d(rm)}{dt} = gct^{g-1} \quad [\text{Eq.25}]$$

The plateau phase, in which rm remains constant, is represented by:

$$\frac{d(rm)}{dt} = 0 \quad [\text{Eq.26}]$$

Finally, the decay phase is characterized by a negative rate, where d represents the rate of mass decay and c continues to modulate the magnitude of the decay. This is expressed as:

$$\frac{d(rm)}{dt} = -dct^{-(d+1)} \quad [\text{Eq.27}]$$

2.4. Neural Force Field

Indeed, the presence of RMS gives rise to a force field that displaces cRFs from their equilibrium positions. In theory, cRFs can be influenced by an infinite number of *rm*, either concurrently or successively, each contributing to the overall perturbation. For instance, a single *rm* located near the target of an impending saccadic eye movement (SEM) can be used to study the convergent form of PNR. Additionally, a virtual *rm* positioned at infinity, aligned with the SEM direction, may also be considered to study its impact in a manner consistent with the translational form of PNR. These configurations can also coexist, enabling the exploration of their interactions within overlapping temporal windows. Such simulation examples underscore the expressiveness and modularity of retinotopic mechanics as a framework, ensuring that different types of PNR can be independently explored and that the model does not inherently favor any specific form of PNR—an issue that has limited previous frameworks described in chapter 1.

3. GENREAL MODEL

In Chapter 1, I provided an overview of three mathematical frameworks and the accompanying models that implement these frameworks, which researchers have used to investigate PNR. In Chapter 2, I introduced the mathematical framework of retinotopic mechanics, highlighting its core advantages. After this I will go on to construct a general model of PNR that implements retinotopic mechanics. This model not only resolves divergent observations in literature such as the focus on translational and convergent accounts—but also uncovers the fundamental principles governing how the brain balances energy expenditure with the need for predictive accuracy. Finally, this general model clarifies the role ϵ l ϕ s play in ensuring that cRFs are appropriately sensitized across the visual space.

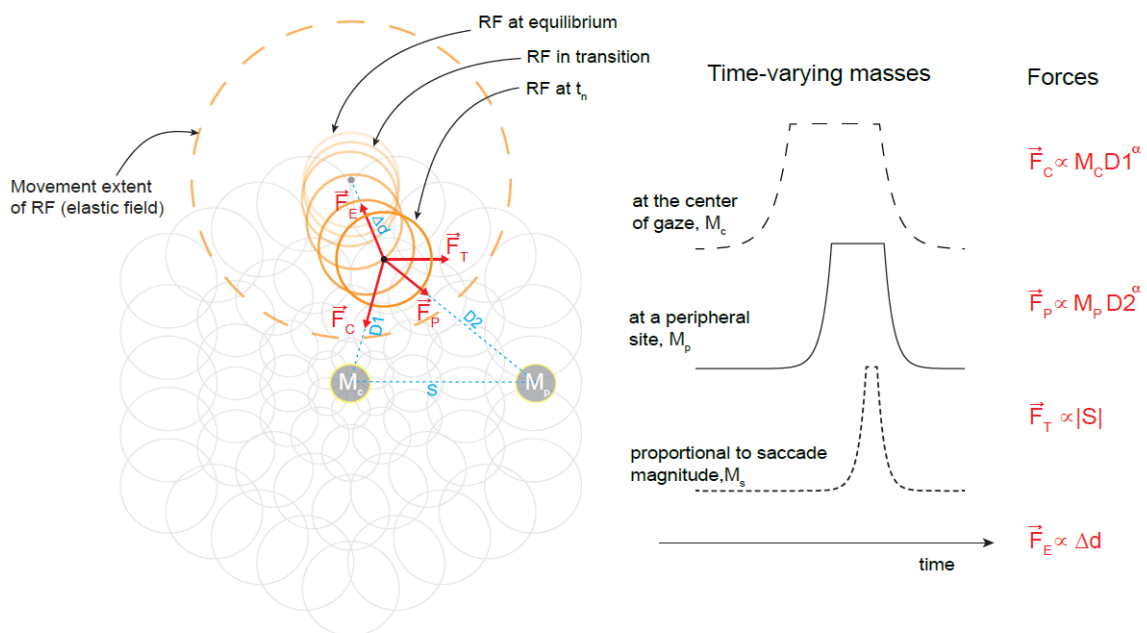


Figure 2. General Model of Remapping Using Retinotopic Mechanics (own representation, Ifedayo-Emmanuel Adeyefa-Olasupo)

3.1. Core Assumption.

The general model will include three forces—centripetal, convergent, and translational—that influence the population of cRFs within distinct but temporally overlapping

windows. We assume the biological system architecture being modeled is a foveated system, where the diameter di of each cRF scales with eccentricity (ecci). Secondly, we assume an adaptive $\varepsilon l\varphi$ which will also scale with eccentricity. Third, we assume that the centripetal force is the first to exert its influence on the cRFs, shifting them toward the current center of gaze, followed by the convergent force, which moves the cRFs toward the saccade target. Finally, the translational force shifts the cRFs in the direction of the impending saccade. In the context of PNR, this means that PNR includes centripetal, convergent, and translational components. Lastly, we assume that the neural force field obeys an inverse-distance law $-\frac{1}{r^{1.6}}$, akin to Newton's law of universal gravitation.

3.1.1. Centripetal Force

Let \vec{f}_c represent the centripetal force that displaces cRF_i from their equilibrium positions toward the central 2° of the visual field. This force is defined in terms of its magnitude and direction, with the expression given by:

$$\vec{f}_c = \begin{cases} k_c \beta \overrightarrow{U_{rm_c}} r m_c r_1^\alpha & \text{for } |r_1| \leq \varepsilon l\varphi \\ 0 & \text{for } |r_1| > \varepsilon l\varphi \end{cases} \quad [\text{Eq.28}]$$

Here $k_c \beta$ denotes the magnitude of the centripetal force, $\overrightarrow{U_{rm_c}}$ is the unit vector in the direction of r_1 , the spatial displacement of cRF_i from rm_c , raised to distance exponent $\alpha - 1.6$. The differential form of the centripetal force is derived by taking the partial derivative with respect to r_1 :

$$d\vec{f}_c = \frac{\partial \vec{f}_c}{\partial r_1} \partial r_1 \quad [\text{Eq.29}]$$

This expression represents the change in the centripetal force as a function of the spatial displacement r_1 . The partial derivative of the centripetal force is given by:

$$\frac{\partial \vec{f}_c}{\partial r_1} = k_c \beta r m_c \frac{\partial}{\partial r_1} (\overrightarrow{U_{rm_c}} r_1^\alpha) \quad [\text{Eq.30}]$$

Applying the power rule to the term r_1^α , results in:

$$\frac{\partial}{\partial r_1} (r_1^\alpha) = \alpha r_1^{\alpha-1} \quad [\text{Eq.31}]$$

Substituting this into the expression for the centripetal force yields the differential form:

$$d\vec{f}_C = k_c \beta r m_c \alpha \overrightarrow{U_{rm_c}} r_1^{\alpha-1} dr_1 \text{ for } |r_1| \leq \varepsilon l \varphi \quad [\text{Eq.32}]$$

This formulation captures the dependence of the differential centripetal force on the spatial displacement r_1 and the exponent α , when cRF_{*i*} is within its $\varepsilon l \varphi_i$, reflecting the dynamics that govern the behavior of cRFs under centripetal forces.

3.1.2. Convergent Force

The centripetal force is followed by the convergent force, where $k_p \beta$ represents the convergent constant. Let $\overrightarrow{U_{rm_p}}$ denote the unit vector in the direction of r_2 , the spatial displacement of cRF_{*i*} from rm_p , raised to α . The convergent force can be expressed as:

$$\vec{f}_p = \begin{cases} k_p \beta \overrightarrow{U_{rm_p}} r m_p r_2^\alpha & \text{for } |r_2| \leq \varepsilon l \varphi \\ 0 & \text{for } |r_2| > \varepsilon l \varphi \end{cases} \quad [\text{Eq.33}]$$

Here the differential form of \vec{f}_p is derived by taking the partial derivative with respect to r_2 :

$$d\vec{f}_P = \frac{\partial \vec{f}_P}{\partial r_2} \partial r_2 \quad [\text{Eq.34}]$$

Analogous to the derivation in the centripetal case, this equation describes the change in the convergent force as a function of r_2 . The partial derivative of the convergent force is given by:

$$\frac{\partial \vec{f}_p}{\partial r_2} = k_p \beta r m_p \frac{\partial}{\partial r_2} (\overrightarrow{U_{rm_p}} r_2^\alpha) \quad [\text{Eq.35}]$$

Applying the power rule for differentiation yields:

$$\frac{\partial}{\partial r_2} (r_2^\alpha) = \alpha r_2^{\alpha-1} \quad [\text{Eq.36}]$$

Substituting this result back into the expression, the differential form becomes:

$$d\vec{f}_p = k_p \beta r m_p \alpha \overrightarrow{U_{rm_p}} r_2^{\alpha-1} dr_2 \text{ for } |r_2| \leq \varepsilon l \varphi \quad [\text{Eq.37}]$$

This formulation highlights the sensitivity of the differential force to the spatial displacement r_2 and α . Furthermore, it captures the progressive attenuation of the force as r_2 approaches $\varepsilon l \varphi$, beyond which the force ceases to exert its influence on cRF_i .

3.1.3. Translational force

Unlike \vec{f}_C and \vec{f}_P , the translational force - \vec{f}_T , exerts its influence due to a mass at infinity rather than at exact spatial extents in visual space. Specifically, the translational force can be expressed as

$$\vec{f}_T = \begin{cases} k_T \beta \overrightarrow{U_{rm_T}} r m_T |s| & \text{for } |s| \leq \varepsilon l \varphi \\ 0 & \text{for } |s| > \varepsilon l \varphi \end{cases} \quad [\text{Eq.38}]$$

Here $k_T\beta$ represents the strength of this force. $\overrightarrow{U_{rm_T}}$ is the unit vector in the direction of rm_T while $|s|$ denotes the magnitude of the impending SEM. The differential form of \vec{f}_T is obtained by taking the partial derivative with respect to $|s|$:

$$d\vec{f}_T = \frac{\partial \vec{f}_T}{\partial |s|} \partial |s| \quad [\text{Eq.39}]$$

This equation describes the infinitesimal change in the translational force as a function $|s|$. Taking the partial derivative yields:

$$\frac{\partial \vec{f}_T}{\partial r_{|s|}} = k_T\beta rm_T \frac{\partial}{\partial |s|} (\overrightarrow{U_{rm_T}} |s|) \quad [\text{Eq.40}]$$

Since $\overrightarrow{U_{rm_T}}$ is a constant unit vector, the derivative simplifies to:

$$\frac{\partial}{\partial |s|} (|s|) = 1 \quad [\text{Eq.41}]$$

Replacing this result into the expression for the differential form, we obtain:

$$d\vec{f}_T = k_T\beta rm_T \overrightarrow{U_{rm_T}} d|s| \quad \text{for } |s| \leq \varepsilon l\varphi \quad [\text{Eq.42}]$$

This formulation shows that the translational force varies linearly with changes in $|s|$, constrained by $\varepsilon l\varphi$. It allows the translational force to govern the motion of cRFs along a saccade direction, with the force weakening once displacement exceeds $\varepsilon l\varphi$.

3.1.4. Spring force (internal dynamics)

The spring force, \vec{f}_s , governs the internal dynamics of cRF_i , in contrast to the external forces that perturb from its equilibrium extent. In its simplest form, this internal dynamic is defined as:

$$\vec{F}_E = \begin{cases} -k\hat{x} & \text{for } |\hat{x}| \leq \varepsilon l\varphi \\ 0 & \text{for } |\hat{x}| > \varepsilon l\varphi \end{cases} \quad [\text{Eq.43}]$$

To express the differential form of the spring force, denoted \vec{f}_s , we first compute its partial derivative with respect to the displacement \hat{x} :

$$d\vec{f}_E = \frac{\partial \vec{f}_E}{\partial \hat{x}} \partial \hat{x} \quad [\text{Eq.44}]$$

This derivative quantifies the incremental change in the spring force with a small variation in \hat{x} . The partial derivative can be expressed as:

$$\frac{\partial \vec{f}_E}{\partial \hat{x}} = \begin{cases} -ks\hat{x} & \text{for } |\hat{x}| \leq \varepsilon l\varphi \\ 0 & \text{for } |\hat{x}| > \varepsilon l\varphi \end{cases} \quad [\text{Eq.45}]$$

Substituting the spring force expression into the partial derivative, and focusing on the case where $|\hat{x}| \leq \varepsilon l\varphi$:

$$\frac{\partial}{\partial \hat{x}} (-ks \hat{x}) = -ks \quad [\text{Eq.46}]$$

Thus, the differential form of the spring force can be expressed as:

$$d\vec{f}_E = -ks \partial \hat{x}, \text{ for } |\hat{x}| \leq \varepsilon l\varphi \quad [\text{Eq.47}]$$

Here this shows that the spring force acts linearly within the defined displacement range. In the case when \hat{x} exceeds $\varepsilon l\varphi$, the spring force is activated and thus providing a restoring influence back to cRF_i equilibrium extent.

3.1.5. Net force

The net force, denoted as \vec{F}_N , represents the cumulative effect of various forces acting on cRF_i. Specifically, this force integrates contributions from the centripetal force \vec{F}_C , convergent force \vec{F}_P , translational force \vec{F}_T , and spring (equilibrium) force \vec{F}_E , reflecting the overall influence on cRF_i. The net force can be mathematically expressed as:

$$\vec{F}_N = \sum_{i=1}^n \vec{F}_i \quad [\text{Eq.48}]$$

To encapsulate the piecewise nature of each force, we incorporate the respective thresholds that dictate the activation of each force. For instance, when any of the individual forces exceed their defined limits - $\varepsilon l\varphi$, the net force contribution from that force may be nullified:

$$\vec{F}_N = \begin{cases} \vec{F}_C + \vec{F}_P + \vec{F}_T + \vec{F}_S & \text{if } r_1 \leq \varepsilon l\varphi, r_2 \leq \varepsilon l\varphi, |s| \leq \varepsilon l\varphi, |\hat{x}| > \varepsilon l\varphi \\ 0 & \text{otherwise} \end{cases} \quad [\text{Eq.49}]$$

Finally, the differential form of the net force can be derived by differentiating each component force:

$$d\vec{f}_N = d\vec{f}_C + d\vec{f}_P + d\vec{f}_T + d\vec{f}_S \quad [\text{Eq.50}]$$

4. RESULTS

4.1.1. Density (sensitivity) readout

To describe the changes in neural sensitivity in response to the displacement of cRF_i , by the net force \vec{F}_N , a bivariate Gaussian function can serve as an effective model. This function, $G(u)$, captures the spatial distribution of sensitivity around cRF_i and can represent the increase or decrease in sensitivity as a response to the displacement. The Gaussian function is given by:

$$G(u) = \frac{1}{2\pi} \exp \left(-\frac{1}{2} u^T u \right) \quad [\text{Eq.51}]$$

Here $\frac{1}{2\pi}$ is a normalization factor that ensures the total area under the Gaussian curve is equal to 1. $-\frac{1}{2} u^T u$ measures the squared Euclidean distance of u from the center of the Gaussian. As u moves further from the center, $G(u)$ decreases rapidly because the exponential function suppresses values that are far from the center. Next, we modify this basic Gaussian function by introducing a bandwidth parameter B , which controls the spread of the Gaussian. This results in the scaled Gaussian function:

$$G_B(u) = B^{-1/2} G(B^{-1/2} u) \quad [\text{Eq.52}]$$

The scaling factor $B^{-1/2}$ is applied to the input u , which stretches or compresses the Gaussian function based on the value of B . A larger B results in a wider Gaussian curve, meaning that the cRF has a broader influence over a larger area. Conversely, a smaller B results in a narrower Gaussian, making the cRF 's influence more localized. The outer $B^{-1/2}$ factor ensures that the total area under the Gaussian remains equal to 1, preserving the properties of a probability density function. Finally, to estimate the overall neural density at a specific retinotopic location rl , we sum up the contributions of multiple neighboring cRF s using the following equation:

$$\widehat{D} (r_l, B) = \frac{1}{n} \sum_{i=1}^n G_B (r_l - r_l^i) \quad [\text{Eq.53}]$$

Here each cRF's contribution to r_l is determined by $G_B(r_l - r_l^i)$, where r_l^i represents the center of the i -th cRF. The function $G_B(r_l - r_l^i)$ calculates how much the i -th RF contributes to the density at r_l , decreasing as the distance between r_l and r_l^i increases. The scaling factor $\frac{1}{n}$ ensures that the final value, which is the sum of contributions from cRF i , is an average (population activity or density).

4.1.2. Putative sensitivity

Changes in density (or sensitivity) at four distinct extents, presumed to map along the radial axis of visual space, was measured as cRF_i were modulated by the influence of \vec{F}_N . In figure 3, the brightest dot represents the foveal outer extent (F_{out}), located to the left of the center of gaze. The second brightest dot represents the foveal inner extent (F_{in}). Next is the peripheral inner extent (P_{in}), positioned left of the saccade target, followed by the peripheral outer extent (P_{out}).

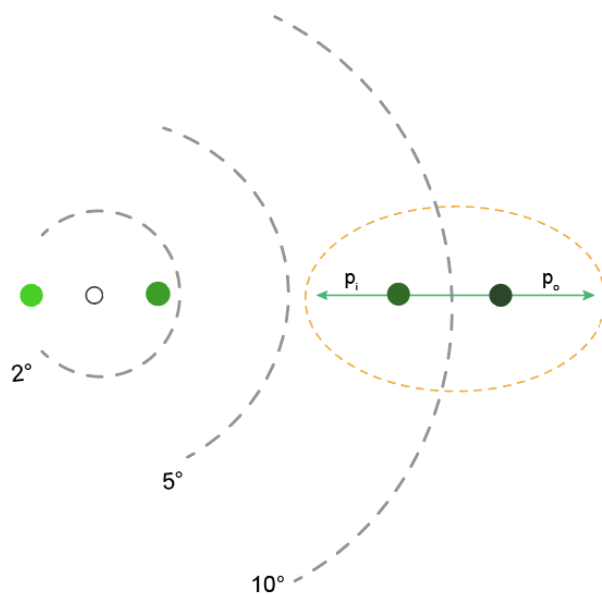


Figure 3. Radial extents sampled. (own representation, Ifedayo-Emmanuel Adeyefa-Olasupo)

4.1.2.1. Density Predictions at Foveal Extents

When cRF_i are subjected to a centripetal force between 150 and 270 ms before the force declines, density levels at F_{in} and F_{out} remain relatively stable, as expected. Following the centripetal force, a convergent force acts to shift cRF_i toward 10 degrees along the radial axis of the visual field. Subsequently, with the activation of a translational force that further shifts cRF_i toward the peripheral region, a rapid decline in density is observed at the foveal extent. Interestingly, F_{out} , being the farthest from the saccade target location, exhibits a slightly higher density level compared to F_{in} , which is closer to the periphery (i.e. the new center of gaze).

4.1.2.2. Density Predictions at Peripheral Extents

Between 150 and 270 ms before the decline of the centripetal force, a noticeable yet modest decline in density levels at p_{in} is observed. Around 240 ms, with the activation of the convergent force directing most—but not all— cRF_i back toward the periphery, a slight rebound in density levels at this location occurs. This is followed by a gradual increase in density as the translational force begins to take effect. At the p_{out} extent, the measured location that is furthest from the centripetal mass, a significant decline in density levels is observed. Around 240 ms, as the convergent force begins to influence cRF_i , a slight rebound in density levels occurs. Interestingly, as the translational force subsequently exerts its influence on cRF_i , this more peripheral extent—though expected to receive resource transfers later from the central region—exhibits a rapid and pronounced increase in density levels compared to the p_{in} extent.

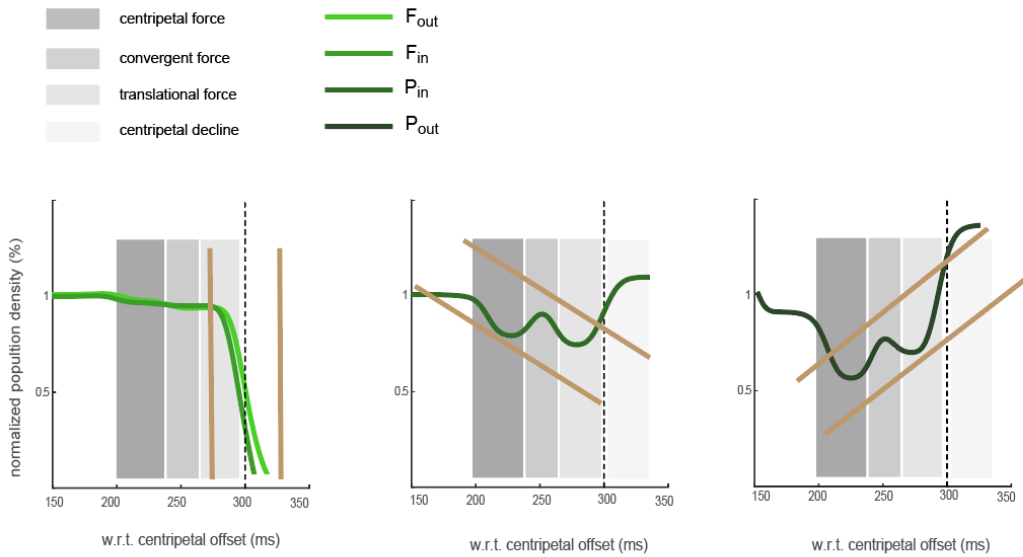


Figure 4. Simulated Changes in density along the radial axis. (own representation, Ifedayo-Emmanuel Adeyefa-Olasupo)

4.1.3. Psychophysical Measurements

In line with predictions from the three-force model, three sets of experiments were conducted with human observers using a cued saccade task. In these experiments, 11 subjects were asked to indicate, via a push button, whether they could detect a faint Gabor probe presented at one of four locations along the radial axis around the time of a SEM. Consistent with simulated predictions, visual sensitivity levels were sustained at F_{in} and F_{out} between 300 to 200 ms before saccade onset at the expense of the P_{in} and P_{out} extents. These observed responses within this temporal window support the foveated system's ability to maintain high sensitivity within the central 2 degrees of the visual field just before a new target is detected at more eccentric extents of visual space. Notably, the centripetal driven sensitivity has not been previously reported. In the post-saccadic window, an interesting effect emerges which the simulation also predicts: the extent that is most distal from the saccade target - F_{out} , exhibits slightly higher density levels than the F_{in} extent.

Before and after the early pre-saccadic window, during which the convergent force is most influential, a transient increase in visual sensitivity is observed at both the P_{in} and P_{out} extents, with a slightly larger increase at P_{in} . Additionally, just before and

after the post-saccadic window, the P_{out} —despite being farther from the central region, where resource transfers are expected to be delayed—shows a faster and more pronounced increase in visual sensitivity compared to P_{in} . This effect arises just before fixation on the new target location, underscoring the complex dynamics in visual sensitivity distribution across the visual field.

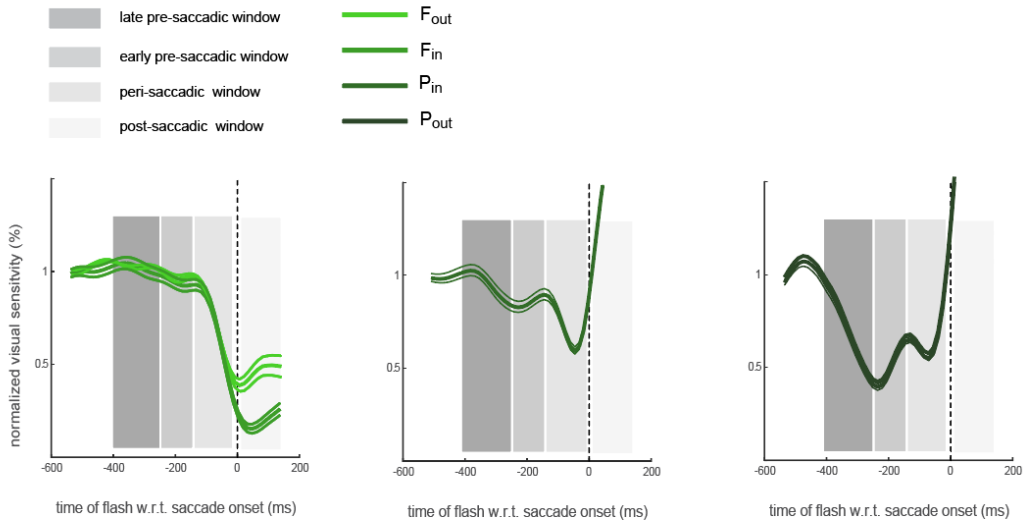


Figure 5. Experimental changes in sensitivity along the radial axis. (own representation, Ifedayo-Emmanuel Adeyefa-Olasupo)

4.1.4. Paradox I

There are two paradoxes that this general model predicts, which are even more apparent in the empirical results. The first paradox is that the probed location furthest from the saccade target, both before and after the saccade is made, should not experience a higher level of sensitivity than the foveal location that is closer to the target. The second paradox is that the peripheral location furthest from where neural resources are being transferred from should not experience a faster and more rapid increase in visual sensitivity compared to the location closer to this energy source. This paradox can be explained by the presence of elastic constraints. Specifically, as the receptive field (cRF) shifts towards the peripheral mass, the cRF located to the left of this mass reaches the boundary of its elastic field and is unable to move further, forcing it to retain its neural energy in the

central region. In contrast, the cRF to the right of the central mass can continue shifting due to the direction of the saccade target, redistributing its neural resources away from the rad-fov-in location. This elastic constraint results in the outer foveal location having a slightly higher level of sensitivity when compared to the foveal location closer to the saccade target. This mechanism is essential for biological systems to ensure that peripheral regions are sufficiently sensitized in the presence of potential aversive stimuli, such as a predator.

4.1.5. Paradox II

The second paradox can be explained by considering the tessellation of classical receptive fields (cRFs) and their elastic fields. Specifically, because of the size of each cRF scales with eccentricity, when cRFs begin to shift towards the peripheral region, larger cRFs deposit greater amounts of neural resources compared to smaller cRFs, even when both types experience the same magnitude of shift. This size difference, combined with the inverse distance law, results in larger cRFs producing greater shifts. This in turn leads to the rad-peri-out location exhibiting a faster and more substantial increase in sensitivity, as it benefits from the larger deposition of neural resources by the larger cRFs just before the eye lands on the target. Notably, since this design principle has only been observed in foveated systems, it would be intriguing to investigate how these effects manifest in other biological systems whose cRF sizes are eccentricity independent.

5. DISCUSSION

The aim of this thesis was to introduce a radically novel mathematical framework that serves as a general framework for understanding active visual processing across different biological systems. Using retinotopic mechanics, I demonstrate that relevant retinotopic brain structures may receive temporally overlapping signals (modelled as forces), causing receptive fields (cRFs) to undergo centripetal, convergent, and translational shifts prior to the onset of saccadic eye movements (SEM). It is plausible that some cRFs exhibit a preference for one form of remapping over another. However, I show that, across retinotopic brain areas, RF shifts are actively mediated by their respective elastic fields (ε l φ s), and these shifts follow an inverse law akin to Newton's law of universal gravitation. While this thesis uncovers the computational relevance of an elastic field, the neurobiological underpinnings of these fields remain unknown. Considering the paradoxes identified in this work, future studies in primates and rodents should aim to replicate these effects and investigate which neurons underlie these paradoxes. It is likely that, for any animal requiring spatial orientation, elastic fields are fundamental to how the organism is able to orient itself within its environment. In fact, in the absence of elastic fields, an animal's ability to perform orientation-mediated tasks—or, in extreme cases, to survive—would be severely compromised.

REFERENCES

1. Spillmann, L. Receptive fields of visual neurons: the early years. *Perception*, 2014; 43(11): 1145–1176.
2. Duhamel, J.R., Colby, C.L., Goldberg, M.E. The updating of the representation of visual space in parietal cortex by intended eye movements. *Science*, 1992; 255(5040): 90–92.
3. Zirnsak, M., Steinmetz, N.A., Noudoost, B., Xu, K.Z., Moore, T. Visual space is compressed in prefrontal cortex before eye movements. *Nature*, 2014; 507(7493): 504–507.
4. Droulez, J., Berthoz, A. A neural network model of sensoritopic maps with predictive short-term memory properties. *Proceedings of the National Academy of Sciences of the United States of America*, 1991; 88(21): 9653–9657.
5. Quaia, C., Optican, L.M., Goldberg, M.E. The maintenance of spatial accuracy by the perisaccadic remapping of visual receptive fields. *Neural Networks*, 1998; 11: 1229–1240.
6. Medendorp, W.P., Tweed, D.B., Crawford, J.D. Motion parallax is computed in the updating of human spatial memory. *Journal of Neuroscience*, 2003; 23: 8135–8142.
7. Wang, X., Zhang, C., Yang, L., Jin, M., Goldberg, M.E., Zhang, M., Qian, N. Perisaccadic and attentional remapping of receptive fields in lateral intraparietal area and frontal eye fields. *Cell Reports*, 2024; 43(3).
8. Keith, G.P., Blohm, G., Crawford, J.D. Influence of saccade efference copy on the spatiotemporal properties of remapping: a neural network study. *Journal of Neurophysiology*, 2010; 103(1): 141–159.
9. Keith, G.P., Crawford, J.D. Saccade-related remapping of target representations between topographic maps: a neural network study. *Journal of Computational Neuroscience*, 2008; 24(2): 157–178.
10. White, R.L. 3rd, Snyder, L.H. A neural network model of flexible spatial updating. *Journal of Neurophysiology*, 2004; 91(4): 1608–1619.

11. Hamker, F.H., Zirnsak, M. V4 receptive field dynamics as predicted by a systems-level model of visual attention using feedback from the frontal eye field. *Neural Networks*, 2006; 19: 1371–1382.
12. Zirnsak, M., Lappe, M., Hamker, F.H. The spatial distribution of receptive field changes in a model of peri-saccadic perception: predictive remapping and shifts towards the saccade target. *Vision Research*, 2010; 50(14): 1328–1337.
13. Hamker, F.H., Zirnsak, M., Calow, D., Lappe, M. The peri-saccadic perception of objects and space. *PLoS Computational Biology*, 2008; 4(2): e31.
14. Nigg JT. Attention-deficit/hyperactivity disorder and adverse health outcomes. *Clin Psychol Rev*. 2013 Mar;33(2):215-28.
15. Marouska M van Ommen, Teus van Laar, Remco Renken, Frans W Cornelissen, Richard Bruggeman, Visual Hallucinations in Psychosis: The Curious Absence of the Primary Visual Cortex, *Schizophrenia Bulletin*, Volume 49, Issue Supplement_1, March 2023, Pages S68–S81, <https://doi.org/10.1093/schbul/sbac140>
16. Adeyefa-Olasupo, I.-E. Visual space curves before eye movement. *bioRxiv*, 2021. <https://doi.org/10.1101/2021.10.13.464140v1>.
17. Gowers, R.P., Richardson, M.J.E. Upcrossing-rate dynamics for a minimal neuron model receiving spatially distributed synaptic drive. *Physical Review Research*, 2023; 5(2): 023095. Publisher: American Physical Society.
18. Végh, J., Berki, A.J. Towards generalizing the information theory for neural communication. *Entropy*, 2022; 24(8).
19. Katkov, M., Tsodyks, M. Statistics of free memory recall. *Physical Review Research*, 2022; 4(3): 033090. Publisher: American Physical Society.
20. Shi, Y.L., Zeraati, R., Levina, A., Engel, T.A. Spatial and temporal correlations in neural networks with structured connectivity. *Physical Review Research*, 2023; 5(1): 013005. Publisher: American Physical Society.
21. Fagerholm, E.D., Dezhina, Z., Moran, R.J., Friston, K.J., Turkheimer, F., Leech, R. Selection entropy: the information hidden within neuronal patterns. *Physical Review Research*, 2023; 5(2): 023197. Publisher: American Physical Society.

22. Nejatbakhsh, A., Fumarola, F., Esteki, S., Toyoizumi, T., Kiani, R., Mazzucato, L. Predicting the effect of micro-stimulation on macaque prefrontal activity based on spontaneous circuit dynamics. *Physical Review Research*, 2023; 5(4): 043211. Publisher: American Physical Society.

23. Golkar, S., Berman, J., Lipshutz, D., Haret, R.M., Gollisch, T., Chklovskii, D.B. Neuronal temporal filters as normal mode extractors. *Physical Review Research*, 2024; 6(1): 013111. Publisher: American Physical Society.

24. Engelken, R., Wolf, F., Abbott, L.F. Lyapunov spectra of chaotic recurrent neural networks. *Physical Review Research*, 2023; 5(4): 043044. Publisher: American Physical Society.

25. Wu, Y.K., Gjorgjieva, J. Inhibition stabilization and paradoxical effects in recurrent neural networks with short-term plasticity. *Physical Review Research*, 2023; 5(3): 033023. Publisher: American Physical Society.

26. Biswas, T., Fitzgerald, J.E. Geometric framework to predict structure from function in neural networks. *Physical Review Research*, 2022; 4(2): 023255. Publisher: American Physical Society.

27. Yao, T., Ketkar, M., Treue, S., Krishna, B.S. Visual attention is available at a task-relevant location rapidly after a saccade. *eLife*, 2016; 5(e18009): 1-12.